


Received: 29 June 2018 | Revised: 31 August 2018 | Accepted: 20 September 2018

DOI: 10.1002/ppap.201800112

## FULL PAPER

PLASMA PROCESSES  
AND POLYMERS

# Metal nanoparticle-hydrogel nanocomposites for biomedical applications – An atmospheric pressure plasma synthesis approach

Hugo Nolan<sup>1</sup> | Daye Sun<sup>1</sup> | Brian G. Falzon<sup>1</sup> | Supriya Chakrabarti<sup>2</sup> |  
Dilli Babu Padmanaba<sup>2</sup> | Paul Maguire<sup>2</sup> | Davide Mariotti<sup>2</sup> | Tao Yu<sup>3</sup> |  
David Jones<sup>3</sup> | Gavin Andrews<sup>3</sup> | Dan Sun<sup>1</sup> 

<sup>1</sup> Advanced Composite Research Group (ACRG), School of Mechanical and Aerospace Engineering, Queen's University Belfast, Belfast BT9 5AH, UK

<sup>2</sup> Nanotechnology and Integrated BioEngineering Centre (NIBEC), Ulster University, Shore Road, Newtownabbey BT37 0PX, UK

<sup>3</sup> School of Pharmacy, Queen's University Belfast, Lisburn Road, Belfast BT9 7BL, UK

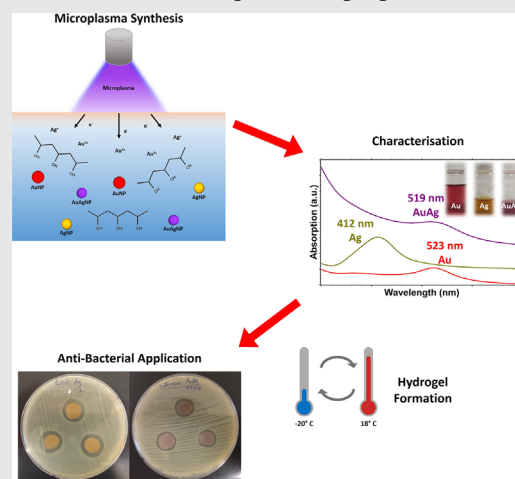
**Correspondence**

Dan Sun, School of Mechanical and Aerospace Engineering, Queen's University Belfast, Belfast BT9 5AH, UK.  
Email: [d.sun@qub.ac.uk](mailto:d.sun@qub.ac.uk)

**Funding information**

Engineering and Physical Sciences Research Council, Grant number: EP/P00394X/1

The development of multifunctional nanocomposite materials is of great interest for various biomedical applications. A popular approach to produce tailored nanocomposites is to incorporate functional nanoparticles into hydrogels. Here, a benign atmospheric pressure microplasma synthesis approach has been deployed for the synthesis of metal and alloy NPs in-situ in a poly (vinyl alcohol) hydrogel. The formation of gold, silver, and gold-silver alloy NPs was confirmed via spectroscopic and microscopic characterization techniques. The properties of the hydrogel were not compromised during formation of the composites. Practical applications of the NP/PVA nanocomposites has been demonstrated by anti-bacterial testing. This establishes AMP processing as a viable one-step technique for the fabrication of NP/hydrogel composites, with potential multifunctionality for a range of biomedical applications.

**KEYWORDS**

anti-bacterial composites, atmospheric pressure microplasma synthesis, biomedical materials, green synthesis, NP/hydrogel composites

## 1 | INTRODUCTION

The application of metal nanoparticles (NPs) in the biomedical field has brought about exciting opportunities

in many areas such as anti-microbial,<sup>[1]</sup> sensing,<sup>[2]</sup> drug delivery,<sup>[3]</sup> and bio-imaging,<sup>[4]</sup> etc. The excellent properties demonstrated by metal NPs in these areas are largely due to their unique size and shape-dependent properties.<sup>[5]</sup>

This is an open access article under the terms of the Creative Commons Attribution License, which permits use, distribution and reproduction in any medium, provided the original work is properly cited.

© 2018 The Authors. *Plasma Processes and Polymers* Published by Wiley-VCH Verlag GmbH & Co. KGaA, Weinheim

Gold (Au) NPs have attracted the widest attention among many other nanomaterials, due to their relative non-toxic nature and promising physicochemical properties. Au has strong affinity to thiol and amine functionalities, which allows them to be surface modified and bind with therapeutic agents via Au-S and Au-N bonding to achieve targeted delivery especially in cancer treatments.<sup>[6]</sup> Immense research efforts have also been made to exploit the functionality of AuNPs in disease detection and diagnosis.<sup>[7]</sup> Additionally, AuNPs also display a strong absorption band in the UV-visible NIR region due to surface plasmon resonance, which makes them interesting materials for biosensing<sup>[8]</sup> and photothermal therapies.<sup>[9]</sup> Silver (Ag) NPs, on the other hand, are one of the most broad spectrum antibacterial agents. AgNPs demonstrate more effective antimicrobial properties than ionic Ag owing to their better permeation/retention effects<sup>[10]</sup> and are effectively used for wound and burn dressings,<sup>[11,12]</sup> surgical instruments,<sup>[13]</sup> and skin grafts.<sup>[14]</sup> Depending on their size, shape, dielectric environment, and mutual electromagnetic interactions among particles in close proximity, AgNPs can also demonstrate localized surface plasmon resonance (LSPR) effects, which enables their applications in photothermal and thermolytic laser therapies.<sup>[15]</sup>

Hydrogels are a grouping of materials which offer excellent biocompatibility which have been employed a wide range of biomedical applications.<sup>[16]</sup> Consisting of a crosslinked network of hydrophilic polymers, hydrogels are highly absorbent and can consist of >90% water. This has seen these materials widely used in contact lenses, wound dressings, drug delivery, and tissue engineering.<sup>[16,17]</sup> Polyvinyl alcohol (PVA) hydrogels are commonly used biomaterials due to their excellent biocompatibility, mechanical strength, and transparency.<sup>[18]</sup>

Incorporation of metal NPs such as AgNPs and/or AuNPs into PVA hydrogel can lead to composite systems that demonstrate mutual benefits of their individual constituent, hence leading to multi-functional materials that hold great promise for various applications, such as anti-microbial, sensing, bioimaging, drug delivery, and many others.<sup>[19,20]</sup>

In recent years, the advantages and the associated potential applications of metal NP/hydrogel composite systems have received great interest from multi-disciplinary research groups. Ser-shen et al. prepared Au-NP hydrogel composites by adding Au nanoshells into N-isopropylacrylamide/acrylamide (NIPAAm/AAm) solutions, and curing of composite was achieved by adding gelation initiator ammonium persulfate and accelerator tetramethylethylenediamine.<sup>[21]</sup> This allowed selective photothermal stimulation of the hydrogel matrix, which could be used in micromechanical applications. Pardo-Yissar et al. also attempted physical incorporation of preformed AuNPs into a gelated PAAm hydrogel to make composites which could be used in electrochemical, quantum, and optical applications.<sup>[22]</sup> AuNPs have also been used as crosslinking agents to form hydrogels which were used in bioprinting applications.<sup>[23]</sup>

Typically, the fabrication of metal NP/hydrogel composites involves introducing pre-formed metal NPs into a polymer matrix, or formation of metal NPs in-situ through chemical reduction. Many of the reducing agents used, such as sodium borohydride (NaBH<sub>4</sub>), hydrazine (N<sub>2</sub>H<sub>4</sub>), or sodium citrate (Na<sub>3</sub>C<sub>6</sub>H<sub>5</sub>O<sub>7</sub>) are toxic and may present significant hazards and biological risks. In addition, chemical reduction methods normally require elevated temperature, long processing time, and complicated cleansing processes.<sup>[24,25]</sup>

To address these issues, naturally occurring “greener” reducing agents (such as plant extracts) have been explored, where phytochemicals, such as ursolic acid, flavonoids, saccharides and proteins, are responsible for the reduction of metal ions.<sup>[26–28]</sup> Despite their better biocompatibility, the extraction for such reducing agents can be complicated. Other alternatives, such as high energy radiation have also been employed for the in-situ fabrication of AuNPs and AgNPs in hydrogel composites.<sup>[10,29]</sup> However, the high cost of the radiation equipment and the potential hazard involved in the radiation processes present challenges to such technology.

Non-thermal Atmospheric Pressure Plasma (AMP), is an emerging technology that is receiving an increasing interest in the biomedical field. When water or other liquids are exposed to AMP, the chemistry induced at the plasma/liquid interface has demonstrated unique opportunities for the synthesis and surface functionalization of various nanomaterials including Si nanocrystals,<sup>[30]</sup> nanocarbon structures,<sup>[31]</sup> metal NPs such as Au and Ag,<sup>[32]</sup> alloy NPs such as Au<sub>x</sub>Ag<sub>1-x</sub>,<sup>[33]</sup> and metal oxide NPs such as F<sub>3</sub>O<sub>4</sub><sup>[34]</sup> and Cu<sub>2</sub>O.<sup>[35]</sup>

Despite numerous inorganic nanostructures have been synthesized/surface functionalized through AMP-water interaction, the in-situ synthesis of polymer-based nanocomposites using AMP is still in its infancy. In previous studies, nanocomposites such as silicon nanocrystal/PEDOT:PSS,<sup>[36]</sup> TiO<sub>2</sub>/PEDOT:PSS,<sup>[37]</sup> and AuNP/PEDOT:PSS<sup>[38]</sup> have been synthesized through AMP-water interaction. The highly reactive plasma chemistry has either modified the inorganic nanomaterial surfaces, or, led to the nucleation/growth of the metal NPs with specific surface charges. As a result, there is enhanced interaction between the NPs with the surrounding polymers, giving rise to highly dispersed nanocomposites with enhanced functionalities (e.g., optical and/or electrical properties). To the best of our knowledge, none of the previous studies have yet explored the one step AMP synthesis of metal NPs/hydrogel biocomposites. The idea is interesting as such material system would possess multi-functionality that can be used for various applications in the biomedical field, such as anti-microbial,<sup>[39]</sup> drug delivery,<sup>[40]</sup> cancer theranostics,<sup>[41]</sup> biosensing,<sup>[42]</sup> etc.

In this study, an AMP approach has been presented for the one-step synthesis of AuNP, AgNP, and AuAg NP/PVA hydrogel bio-nanocomposites. The as prepared materials have been characterized for their materials properties and their antibacterial properties have been demonstrated.

## 2 | EXPERIMENTAL SECTION

### 2.1 | Materials

Silver nitrate ( $\text{AgNO}_3$ , >99%), chloroauric acid trihydrate ( $\text{HAuCl}_4 \cdot 3\text{H}_2\text{O}$ , >99.9%), and PVA (99+ % hydrolyzed) were purchased from Sigma–Aldrich and used as-received. All solutions were made using 18.2 M $\Omega$  distilled water. PVA solutions were formed by dissolving the appropriate amount of polymer granulate in water and mixing at 85 °C for 2 h.

### 2.2 | Atmospheric pressure plasma set-up

A schematic of the AMP system is presented in Figure 1. A stainless-steel capillary (inner diameter 250  $\mu\text{m}$ ) was positioned approx. 1 mm above the PVA/salt solution (20 ml) surface. A flow of helium (He) gas (25 sccm) was maintained through the capillary. The capillary was connected to an external circuit controlled by a power supply with a Pt wire forming the anode in the PVA/salt solution. The AMP was ignited by applying a voltage of approx. 2 kV and the current was regulated to maintain a constant 2 mA throughout. The voltage then stabilized at approx. 0.7 kV during the experiment.

### 2.3 | Sample preparation

To produce metal NP/PVA composite samples, metal salt precursors were first dissolved into 4% PVA to make a homogenous mixture. The solution was then subjected to AMP treatment under constant magnetic stirring. For AuAg samples, both salts were first mixed together in PVA solution before AMP treatment. Aqueous AgNPs and AuNPs water colloids (PVA-free) were also prepared by dissolving metal salt in distilled water and carrying out the AMP treatment following the same processing conditions. Table 1 lists the precursor concentration used for all samples. The Ag precursor concentrations is in line with research by Oliveira et al.<sup>[10]</sup> in wound dressing applications. Mixed AuAg

samples were kept at the ratio of  $[\text{Au}]:[\text{Ag}]$  1:4 to ensure no precipitation of AgCl due to an overabundance of  $\text{Cl}^-$ .<sup>[33]</sup> All samples were AMP-treated for 10 min.

### 2.4 | Characterization

UV-vis spectra of all liquid samples were recorded in a Perkin-Elmer Lambda 650 spectrometer. Fourier Transform Infrared (FTIR, Thermo Scientific, Nicolet iS5 model equipped with ATR 1D5). The XPS results were obtained from a Kratos Axis Ultra XPS system (monochromatic Al  $K\alpha$  X-rays, 1486 eV) using a current of 10 mA and a voltage of 15 kV, respectively. The chamber base pressure was  $1 \times 10^{-9}$  mbar. The samples were drop casted on intrinsic silicon wafer and dried completely. High-resolution (instrument resolution of 0.05 eV) XPS spectra including C 1s, Au 4f peaks, and Ag 3d were performed at and a pass energy of 40 eV. The C 1s peak located at 284.5 eV was used for the calibration of the obtained spectra. The software package CasaXPS was employed for the data analysis. Fitting of spectral components for core levels was carried out in accordance with values provided in the Handbook of XPS and the online resource “XPSfitting.com.”<sup>[43,44]</sup> The dimensions and size distributions of NPs were analyzed using Transmission Electron Microscopy (TEM, Philips Tecnai F20D). All liquid samples were diluted (by a factor of 5) before drop-casting onto TEM sample grids. Particle size distribution was analyzed using “FIJI” software package. Images were converted to binary black and white with a threshold set to eliminate the background noise. Particle sizes were automatically measured using the built-in “Particle Size” analysis function in the software package. Over 100 particles were analyzed for each sample type, ensuring meaningful statistics.

Hydrogel samples were produced for mechanical and anti-bacterial tests by subjecting NP/PVA solutions to freeze/thaw cycling to crosslink the PVA molecules.<sup>[45]</sup> Specifically, samples were poured into PTFE moulds, frozen at  $-20$  °C for 14 h and then thawed at 18 °C for 10 h. Four freeze/thaw cycles were carried out, resulting in cylindrical composite samples approximately  $9 \times 14$  mm in size. Representative samples of these hydrogels are shown in Figure 2(b).

Compression tests were carried out using a Lloyds LRX series materials testing machine. Composite samples were compressed at a rate of  $2 \text{ mm min}^{-1}$  to a maximum compression of 5 mm. The compressive modulus for each sample was measured by recording the initial slope of the compression curve up to 20% strain.<sup>[46]</sup> The values reported are averaged over five individual samples. The sample microstructure (morphology, porosity, etc.) was analyzed using a Scanning Electron Microscope (SEM) (Joel 6500 FEG). Samples were freeze-dried, dipped in liquid nitrogen and cryofractured to expose the internal polymer structure. Gold was sputtered onto the fractured sample surfaces before SEM observation.

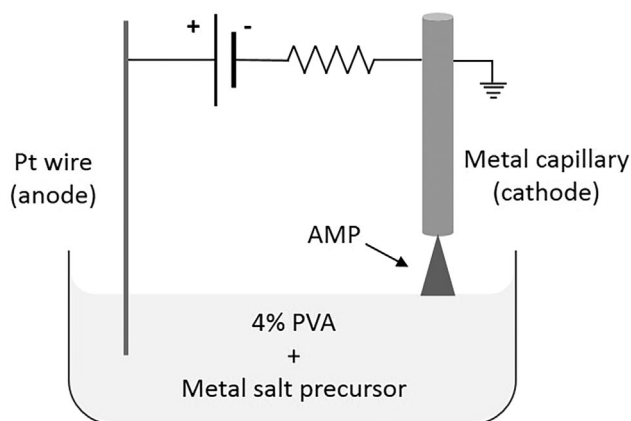


**FIGURE 1** Schematic of the AMP experimental set-up

**TABLE 1** Metal NP/PVA samples discussed in this study

NP type	Au		Ag		AuAg	
Initial precursor concentration	0.1 mM	0.2 mM	0.6 mM	1.2 mM	0.1:0.4 mM (Au:Ag)	0.2:0.8 mM (Au:Ag)
Sample name	Au0.1	Au0.2	Ag0.6	Au1.2	AuAg0.1:0.4	AuAg0.2:0.8

All samples were APM-treated for 10 min.

Dynamic Scanning Calorimetry (Perkin-Elmer DSC 6 instrument) was performed to confirm the crystallinity of the samples prepared. Freeze dried hydrogel samples were heated at a rate of  $20\text{ }^{\circ}\text{C min}^{-1}$  in the temperature range from 30 to  $240\text{ }^{\circ}\text{C}$ , under  $\text{N}_2$  atmosphere. Swelling ratios were determined using the following equation,

$$\text{Swelling ratio} = \frac{m_w}{m_d} \quad (1)$$

where the wet mass ( $m_w$ ) was measured by immersing composite hydrogel samples in water for 3 days, blotting excess water on filter paper and measuring the mass. The dried mass ( $m_d$ ) was measured by drying the samples in a vacuum oven at  $60^{\circ}$  until no further weight loss. Three individual samples were measured for each sample type. The anti-bacterial performance of the as prepared freeze-thawed composite samples was tested against gram-positive *Staphylococcus aureus* (*S. aureus*) and gram-negative *Escherichia coli* (*E. coli*). Composite samples were placed on agar plates which had previously been swabbed with 500 000 bacteria and there were then incubated in LBB broth overnight at  $37\text{ }^{\circ}\text{C}$ . The length of the inhibition zone surrounding the samples was measured and average length measured from three samples were used to determine anti-bacterial activity.

### 3 | RESULTS AND DISCUSSION

#### 3.1 | Spectroscopic analysis of NP/PVA solutions

AMP treatment of  $\text{HAuCl}_4/\text{PVA}$  and  $\text{AgNO}_3/\text{PVA}$  solutions results in a color change of all solutions (see Figure 2[a]), which remain stable and well dispersed even after 2 months. The yellow color of the AMP-treated solution is typical of

colloidal silver, while the appearance of the red/purple solution implies the formation of AuNPs with certain size distribution.

UV-vis absorption spectroscopy (Figure 3) confirmed the presence of Au and Ag NPs in the respective solutions. Specifically, AMP-treated  $\text{HAuCl}_4/\text{PVA}$  solutions exhibit a Surface Plasmon Resonance (SPR) peak at 523 nm, corresponding to the SPR of AuNPs. Similarly, the AMP-treated  $\text{AgNO}_3/\text{PVA}$  solutions display a peak at 413 and 412 nm for Ag0.6 and Ag1.2, respectively. These correspond to the SPR peaks of AgNPs, which are typically found at  $>400\text{ nm}$ .<sup>[47]</sup> The presence of other Ag nanomaterials such as Ag-halide structures can be discounted, as these materials display considerably different UV-vis absorption characteristics to AgNPs.<sup>[48]</sup> The AuAg/PVA solutions demonstrate weak absorption peaks at 509 and 519 nm for AuAg0.1:0.4 and AuAg0.2:0.8, respectively.

Since the physical mixture of different metal NPs will lead to two distinct absorption peaks,<sup>[49]</sup> the single absorption peaks exhibited by our AuAg/PVA samples with their peak position shifted toward the Ag characteristic peak, suggests the formation an bimetallic phase.<sup>[50,51]</sup> Silver and gold both have fcc structures with lattice parameters of 0.408 and 0.409 nm, respectively. The small lattice constant mismatch and identical crystal structures of both metals facilitates the formation of alloyed NPs.<sup>[39]</sup> The SPR of AuAg alloyed NPs shifted from the SPR of pure Au toward the SPR of pure Ag with addition of silver salt precursor.

This suggestion of alloying of the AuAg samples is further supported by XPS analysis. Deconvolution of the Au4f and Ag3d peak regions revealed the positions of the various spectral contributions, as summarized in Table 2. This shows that the Au4f 7/2 component shifts to higher binding energies for AuAg samples compared to Au. Similarly, the Ag3d 5/2 component shifts to lower binding energies in AuAg samples compared to pure Ag. Both of these behaviors have been

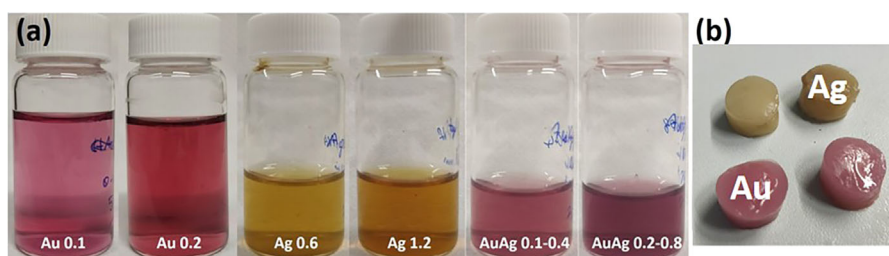


**FIGURE 2** (a) Plasma treated AuNP, AgNP, or AuAgNP/PVA solutions with different precursor concentration. (b) Representative images of Au and Ag/PVA hydrogels



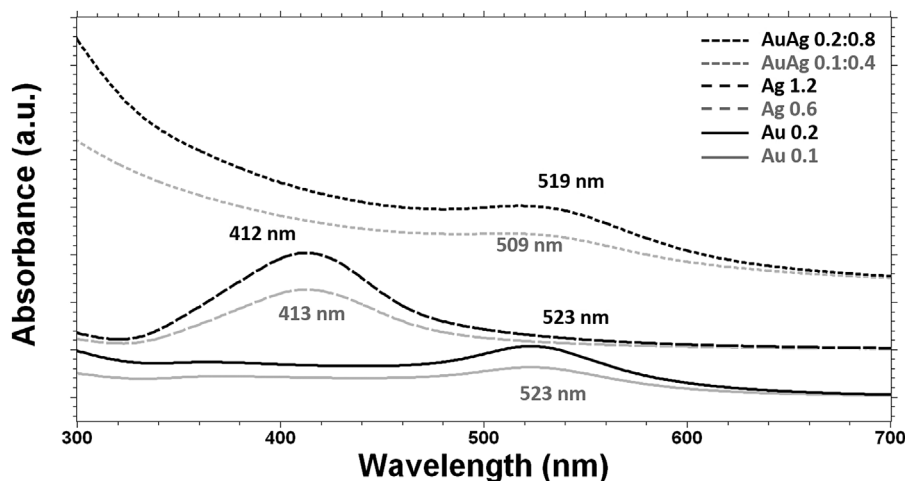


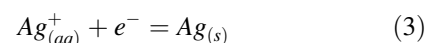
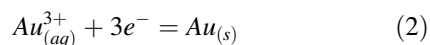
**FIGURE 3** UV-vis spectra for all metal NP samples in PVA. Peak absorption wavelengths are labeled

**TABLE 2** Au and Ag core level peak positions for Au, Ag, and AuAg samples

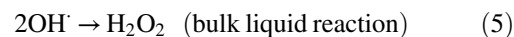
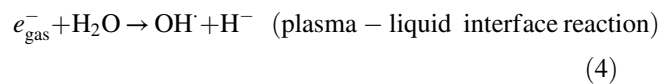
Sample	Au4f 7/2 (eV)	Ag3d 5/2 (eV)
Au0.1	82.9	–
AuAg 0.1:0.4	83	366.8
AuAg 0.2:0.8	83	367
Ag0.6	–	367.3

shown to arise due to alloying of the materials,<sup>[52–54]</sup> indicating the formation of alloyed structures here. More detailed XPS analysis can be found in the Supplementary Information.

Owing to the presence of multiple substances in the reaction system ( $\text{HAuCl}_4$ ,  $\text{AgNO}_3$ ,  $\text{H}_2\text{O}$ , PVA), it is likely that multiple reaction mechanisms have contributed to the formation of the AuAg alloyed NPs. The dissociated metal ions can gain electrons from the AMP the following half-cell reactions:<sup>[33]</sup>



On the other hand, our previous work suggested that the energetic electrons from the AMP may interact with water triggering the following reactions;<sup>[55]</sup>



where reaction (1) represents dissociative electron attachment in the vicinity of the liquid/vapor water interface by electrons from the plasma, producing  $\text{H}^-$  that has a very short lifetime and quickly react with water molecules without participating the AuNP synthesis.  $\text{OH}^\cdot$  has a lifetime in the nanosecond range can quickly react to produce  $\text{H}_2\text{O}_2$ , which has a lifetime of several days, reaction (2). Free electrons that do not contribute to reaction (1) can reach the bulk of the liquid, either to contribute to the reduction of AgNPs, or forming hydrated electrons and produce  $\text{OH}^\cdot$  and

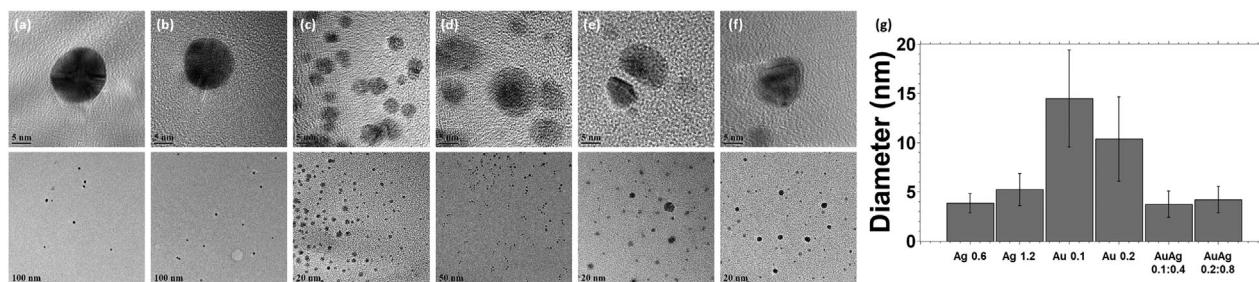


**FIGURE 4** TEM images of (a) Au0.1, (b) Au0.2, (c) Ag0.6, (d) Ag1.2, (e) AuAg0.1:0.4, and (f) AuAg0.2:0.8 at different magnifications. (g) NP sizes for each sample

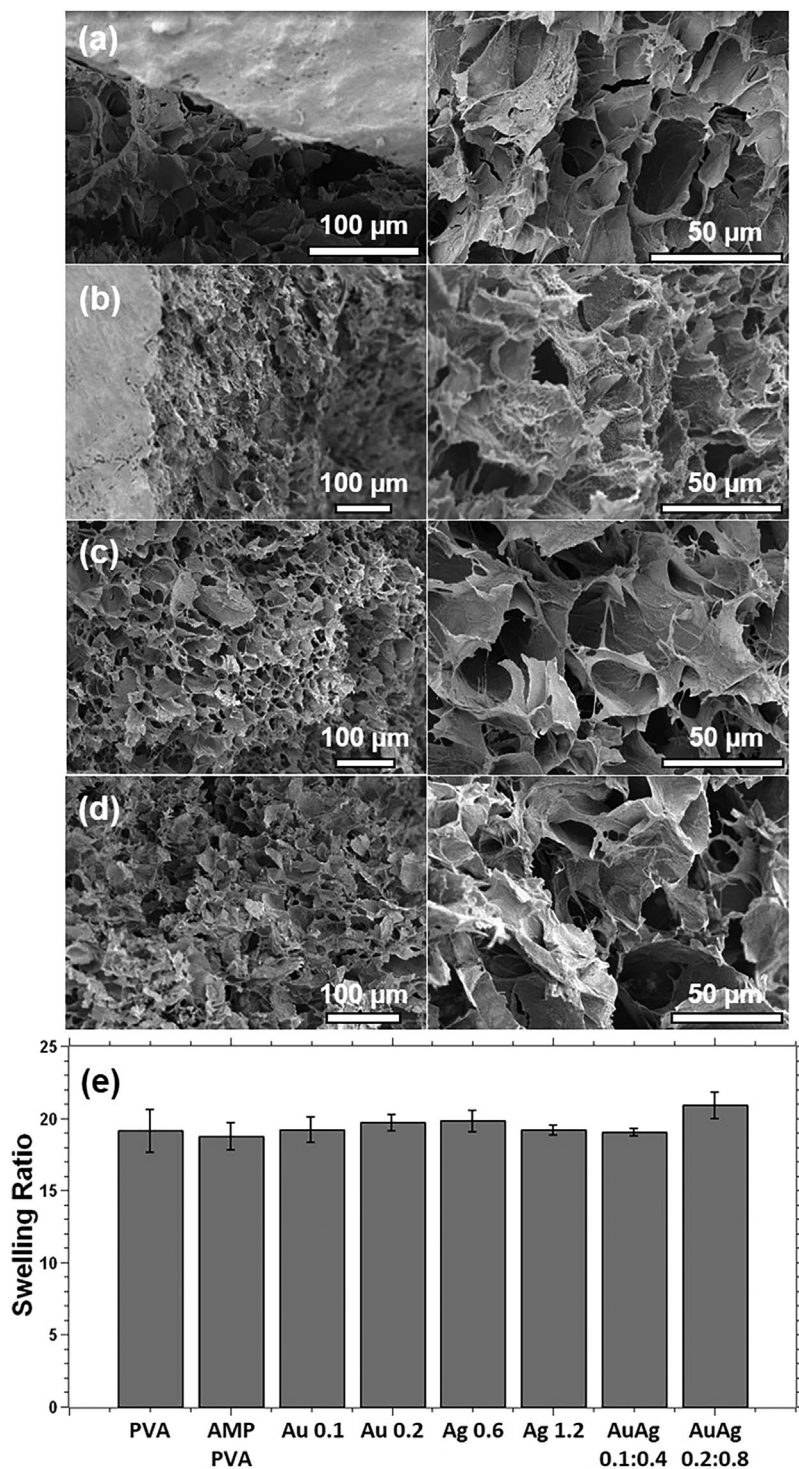
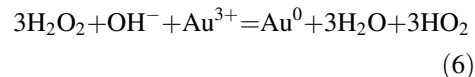


**FIGURE 5** SEM images of (a) PVA, (b) Au 0.2, (c) Ag 1.2, and (d) AuAg 0.1:0.4 hydrogels at different magnifications

$H^-$  in water. It was also found that the AuNPs cannot be synthesized in the absence of water, hence water molecules or corresponding ions ( $OH^-$  or  $H^+$ ) should play a role in the reduction of the gold salt precursor. The role of hydrogen peroxide in the reduction of  $HAuCl_4$  has been extensively discussed in the literature,<sup>[56]</sup> and has been discussed in

greater detail in our previous work on AMP synthesis of AuNPs, in which the following reaction pathway is proposed:<sup>[57]</sup>



In contrast to the results shown thus far, AMP synthesized NPs in water (no PVA) showed much more varied results. AMP treatment of  $AgNO_3$  in water necessitated an oxygen-free environment to achieve any color change in solution, as AgNPs are highly sensitive to atmospheric oxygen.<sup>[58,59]</sup> The AuNP and AuAgNP water colloids demonstrated different pigmentation compared to the corresponding PVA colloids. Furthermore, the water colloids exhibited UV-vis absorption spectra with asymmetric and broader peaks compared to the PVA colloids (see Supporting Information [SI]), indicating variation in NP size or agglomeration.<sup>[57]</sup>

### 3.2 | Microscopic analysis

Metal NP dimensions and size distribution were studied using TEM. Representative images, shown in Figure 4, indicate that NPs synthesized in PVA are well-dispersed with no evidence of clusters or agglomeration. In contrast to previous reports on Au or AgNP synthesized in water, which demonstrate other geometries such as rods, cones, stars, or cubes,<sup>[57]</sup> our Au and Ag synthesized in PVA are largely spherical in shape, while the AuAg/PVA particles consist of distorted round shapes. It is suggested that one of the roles of PVA is to serve as capping agent to protect metal NPs from aggregation in solution.<sup>[60]</sup> The ability of PVA to protect AgNPs from water prevented the rapid degradation/oxidation of silver when in contact with water.<sup>[61,62]</sup> Kyrychenko et al.,<sup>[63]</sup> through molecular dynamics simulation, have discovered that PVA molecules adsorb onto the AgNP surface through multiple non-covalent interactions, among which non-covalent bonding of the hydroxyl groups plays a key role in stabilising the AgNPs. The polymer molecules assembled on the metal NP cores at their nucleation stage, impede the interaction between reactive species with metal nucleus, and hence modulate the NP growth, morphology, and shape.

The size distribution of the samples is shown in Figure 4 (g). Ag0.6 and Ag1.2 showed particles approx. 4–5 nm in

diameter, Au0.1 and Au0.2 were in the range of 10–15 nm in diameter, AuAg0.1:0.4 and AuAg0.2:0.8 both exhibit diameters of approx. 4 nm. Figure 4(a–f) shows a selection of TEM images at high and lower magnification, highlighting the typical shapes of each NP sample type.

SEM of freeze-dried samples (Figure 5) found no significant difference in the morphology of the NP/PVA hydrogels compared to that of pure PVA. The swelling behavior of the various samples is presented in Figure 5(e). The swelling ratios are fairly constant for all samples, which can be correlated well to the similar porosities shown by all the samples.

### 3.3 | Mechanical properties

The compressive moduli of all the samples are presented in Figure 6(a). AMP-treated PVA hydrogels show a significant increase in compressive modulus compared to untreated PVA. FTIR was used to probe the nature of the molecular chemistry in the PVA composite samples.

However, no significant differences were observed in the spectral features for pristine PVA, plasma treated PVA and NP/PVA composites, see Figure 6(b). The presence of plasma induced chemistry such as  $H_2O_2$  and other reactive radicals such as  $O^\cdot$ ,  $H^\cdot$ ,  $OH^\cdot$ , may have caused increased H-bonding in the PVA. This, however, would be hard to prove; as any change in the H-bonding environment will not elicit a measurable change in the corresponding FTIR peak.

H-bonding is manifested in the broad peak at approx.  $3300\text{ cm}^{-1}$ , which is associated with the O–H stretch in PVA.<sup>[64]</sup>

On the other hand, the AMP treated NP/PVA samples show a more complex picture, with a reduction in compressive modulus compared to that of AMP-treated pure PVA (but higher than that of pure PVA). Electrolytes are known to disrupt the inter- and intra-molecular hydrogen bonding in PVA.<sup>[65]</sup> However, the synthesized metal NPs could serve as physical crosslinkers that reinforce the composite structure.<sup>[66]</sup> In addition, the subsequent physical crosslinking

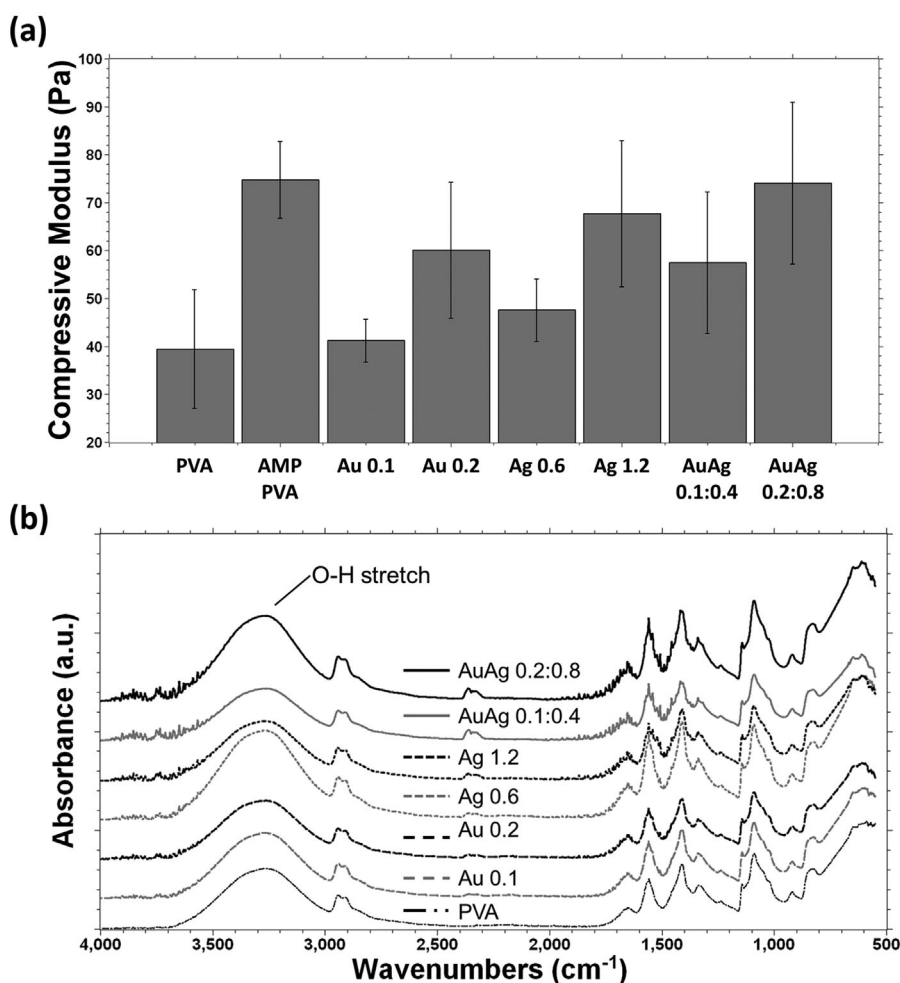


**FIGURE 6** (a) Compressive modulus for and (b) FTIR spectra for PVA and NP/PVA samples



process during the repeated freezing–thawing cycles may involve formation of crystallinities, liquid–liquid phase separation processes, and chains entanglements; which may also contribute to the composite compressive properties. DSC analysis was carried out to assess the thermal behavior of PVA and metal NP/PVA composites. It was found that AMP treatment had a negligible effect on either the glass transition temperature ( $T_g$ ) or the degree of crystallinity in cross-linked composites, see SI.

At this stage, it is difficult to draw solid conclusion how different factors (metal salt, AMP treatment/metal NP formation, freezing–thawing) could have contributed to the crosslinking of PVA. The resulting compressive moduli of the composite samples maybe due to of a combination of very complex mechanisms developed throughout the hydrogel composite fabrication process, and this will be a subject for future study.

### 3.4 | Anti-bacterial properties

The activity of the various metal NP/PVA composites against *E. coli* and *S. aureus* is shown in Figure 7(a and b), respectively. The inhibition zones (summarized in Figure 7 [c]) are clearly visible around Ag containing samples, while not for others. AgNP/PVA composites were effective against both *E. coli* and *S. aureus*, and increased Ag concentration resulted in greater antibacterial effects toward

*E. coli* but similar effects toward *S. aureus*. AuNP/PVA composites showed no antibacterial behavior against either bacterial strain. The AuAgNP/PVA composites formed an inhibition zone in both bacteria strains, but with lower antibacterial activity compared to that of the AgNP/PVA composites. This can be attributed lower silver salt precursors used (e.g., when comparing AuAg 0.1:0.4 sample with Ag 0.6 sample), and the fact that only a fraction of the alloyed particles consist of Ag.

The potential pathways toward the overall antibacterial effect of the Ag containing samples are as follows. It is possible that there are some residual silver ions present in the samples which can partly contribute to the antibacterial effect. The presence of AgNPs (those on the sample surface, or leached out of the sample) is also likely to offer strong antimicrobial effect due to their increased surface area.<sup>[67]</sup> The generation of Reactive Oxygen Species (ROS) by the AgNPs is the primary source of their antibacterial behavior.<sup>[68]</sup> When in contact with bacterial, the surface electronic effects of AgNPs allow them to target the bacterial membrane and to destabilize the plasma membrane potential that leads to the depletion of the levels of intracellular adenosine triphosphate, resulting in the death of bacterial cells.<sup>[69]</sup> The hydrated nature of the nanocomposite samples in this study allows migration of ROS from within the nanocomposite to the periphery, where interaction with bacterial cells takes place.

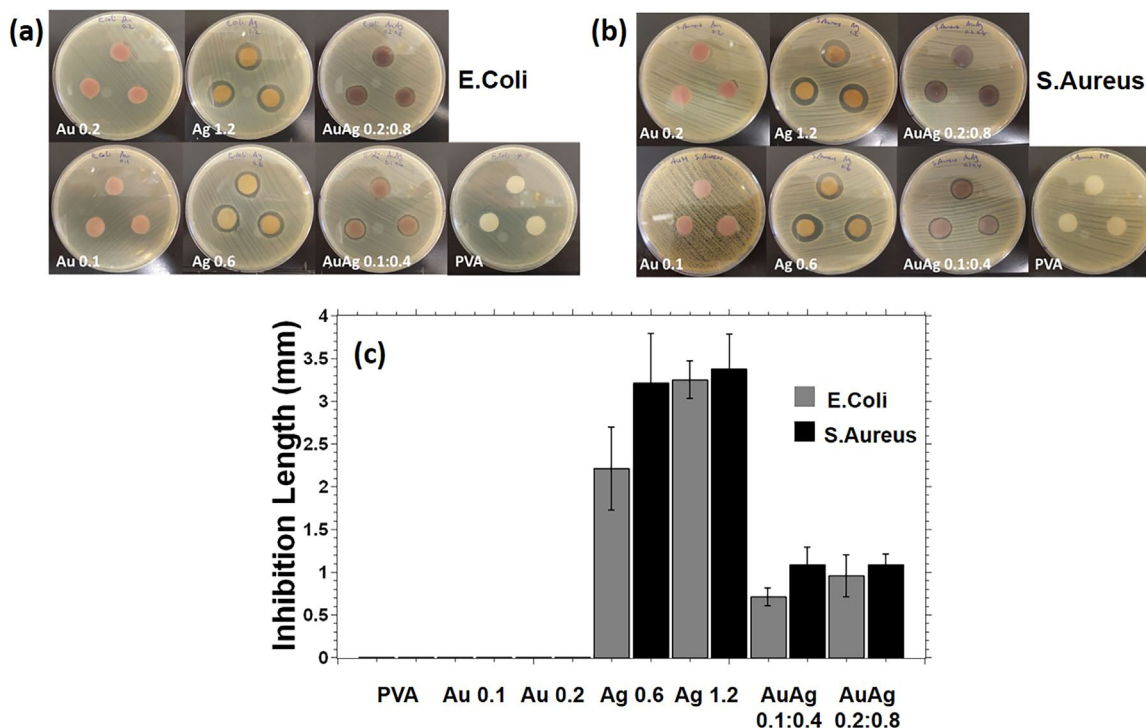


**FIGURE 7** Anti-bacterial tests of NP/PVA composites against (a) *E. coli* and (b) *S. aureus*. (c) Inhibition lengths corresponding to (a) and (b)



## 4 | CONCLUSION

AMP processing has been successfully employed to synthesize Au, Ag, and AuAg alloyed NPs in-situ in PVA hydrogels to produce multi-functional composites for biomedical applications. In this study, PVA serves as a capping agent which prevents NP agglomeration. The presence of PVA molecules could also impede the further interaction between the NP nuclei with the reactive species, hence affecting NP crystal growth kinetics as well as the resulting NP size and morphology. The slower NP growth rate greatly contributes to the better controlled NP shape and particle size distribution. The compressive moduli of the synthesized composite samples have not been compromised by the AMP processing as compared to pristine PVA. All composite samples containing AgNPs exhibit anti-bacterial behavior against both *E. coli* and *S. aureus*.

This study demonstrates that AMP processing is a viable route toward facile synthesis of metal NP/hydrogel composites. The presence of multi-functional Au and Ag NPs in the hydrogel composites will also open great opportunities for other biomedical applications such as drug delivery, sensing, bioimaging, cancer treatment, etc. With the establishment of this novel platform technology, further research has been planned in these areas to further exploit the wide applications of the materials.

## ACKNOWLEDGMENT

The authors would like to acknowledge EPSRC (EP/P00394X/1) for funding support.

## ORCID

Dan Sun  <http://orcid.org/0000-0002-5100-2749>

## REFERENCES

- [1] M. Moritz, M. Geszke-Moritz, *Chem. Eng. J.* **2013**, 228, 596.
- [2] S. Chen, R. Yuan, Y. Chai, F. Hu, *Microchim. Acta* **2013**, 180, 15.
- [3] L. Zhang, D. Pornpattananangkul, C.-M. J. Hu, C.-M. Huang, *Curr. Med. Chem.* **2010**, 17, 585.
- [4] O. S. Wolfbeis, *Chem. Soc. Rev.* **2015**, 44, 4743.
- [5] B. Akbari, M. Pirhadi Tavandashiti, M. Zandrahimi, *Iran. J. Mater. Sci. Eng.* **2011**, 8, 48.
- [6] S. Bhattacharyya, R. A. Kudgus, R. Bhattacharya, P. Mukherjee, *Pharm. Res.* **2011**, 28, 237.
- [7] D. Huo, J. Ding, Y. X. Cui, L. Y. Xia, H. Li, J. He, Z. Y. Zhou, H. W. Wang, Y. Hu, *Biomaterials* **2014**, 35, 7032.
- [8] J.-C. Tinguely, I. Sow, C. Leiner, J. Grand, A. Hohenau, N. Felidj, J. Aubard, J. R. Krenn, *BioNanoScience* **2011**, 1, 128.
- [9] X. Huang, P. K. Jain, I. H. El-Sayed, M. A. El-Sayed, *Lasers Med. Sci.* **2008**, 23, 217.
- [10] R. N. Oliveira, R. Rouzé, B. Quilty, G. G. Alves, G. D. A. Soares, R. M. S. M. Thiré, G. B. McGuinness, *Interface Focus* **2014**, 4, 20130049.
- [11] T. Maneerung, S. Tokura, R. Rujiravanit, *Carbohydr. Polym.* **2008**, 72, 43.
- [12] J. Chen, C. M. Han, X. W. Lin, Z. J. Tang, S. J. Su, *Zhonghua Wai Ke Za Zhi* **2006**, 44, 50.
- [13] D. M. Eby, H. R. Luckarift, G. R. Johnson, *ACS Appl. Mater. Interfaces* **2009**, 1, 1553.
- [14] C. Bianco, G. Adami, M. Crosera, F. Larese, S. Casarin, C. Castagnoli, M. Stella, G. Maina, *Burns* **2014**, 40, 1390.
- [15] L. Wei, J. Lu, H. Xu, A. Patel, Z.-S. Chen, G. Chen, *Drug Discov. Today* **2015**, 20, 595.
- [16] E. Caló, V. V. Khutoryanskiy, *Eur. Polym. J.* **2015**, 65, 252.
- [17] E. M. Ahmed, *J. Adv. Res.* **2015**, 6, 105.
- [18] M. I. Baker, S. P. Walsh, Z. Schwartz, B. D. Boyan, *J. Biomed. Mater. Res. B Appl. Biomater.* **2012**, 100B, 1451.
- [19] S. Kumaraswamy, S. H. Mallaiiah, *Radiat. Eff. Defects Solids* **2016**, 171, 869.
- [20] A. C. Manikas, A. Papa, F. Causa, G. Romeo, P. A. Netti, *RSC Adv.* **2015**, 5, 13507.
- [21] S. R. Sershen, S. L. Westcott, N. J. Halas, J. L. West, *Appl. Phys. Lett.* **2002**, 80, 4609.
- [22] V. Pardo-Yissar, R. Gabai, A. N. Shipway, T. Bourenko, I. Willner, *Adv. Mater.* **2001**, 13, 1320.
- [23] A. Skardal, J. Zhang, L. McCoard, S. Oottamasathien, G. D. Prestwich, *Adv. Mater.* **2010**, 22, 4736.
- [24] M. Grzelczak, J. Pérez-Juste, P. Mulvaney, L. M. Liz-Marzán, *Chem. Soc. Rev.* **2008**, 37, 1783.
- [25] K. Varaprasad, Y. M. Mohan, S. Ravindra, N. N. Reddy, K. Vimala, K. Monika, B. Sreedhar, K. M. Raju, *J. Appl. Polym. Sci.* **2010**, 115, 1199.
- [26] S. Chandran, V. Ravichandran, S. Chandran, J. Chemmunda, B. Chandarshekar, *J. Appl. Res. Technol.* **2016**, 14, 319.
- [27] H. Tyagi, A. Kushwaha, A. Kumar, M. Aslam, *AIP Conf. Proc.* **2011**, 1349, 419.
- [28] J. Bhaumik, N. S. Thakur, P. K. Aili, A. Ghanghoriya, A. K. Mittal, U. C. Banerjee, *ACS Biomater. Sci. Eng.* **2015**, 1, 382.
- [29] S. Kumaraswamy, S. H. Mallaiiah, *Radiat. Eff. Defects Solids* **2016**, 171, 869.
- [30] S. Askari, I. Levchenko, K. Ostrikov, P. Maguire, D. Mariotti, *Appl. Phys. Lett.* **2014**, 104, 163103.
- [31] Y. Shimizu, A. C. Bose, T. Sasaki, D. Mariotti, K. Kirihara, T. Kodaira, K. Terashima, N. Koshizaki, *Trans. Mater. Res. Soc. Jpn.* **2006**, 31, 463.
- [32] C. Richmonds, R. M. Sankaran, *Appl. Phys. Lett.* **2008**, 93, 131501.
- [33] T. Yan, X. Zhong, A. Evelyn Rider, Y. Lu, S. A. Furman, K. (Ken) Ostrikov, *Chem. Commun.* **2014**, 50, 3144.
- [34] R. Wang, S. Zuo, W. Zhu, J. Zhang, J. Fang, *Plasma Process. Polym.* **2014**, 11, 448.
- [35] C. Du, M. Xiao, *Sci. Rep.* **2014**, 4, 7339.
- [36] S. Mitra, S. Cook, V. Švrček, R. A. Blackley, W. Zhou, J. Kovač, U. Cvelbar, D. Mariotti, *J. Phys. Chem. C* **2013**, 117, 23198.
- [37] Y. Liu, D. Sun, S. Askari, J. Patel, M. Macias-Montero, S. Mitra, R. Zhang, W.-F. Lin, D. Mariotti, P. Maguire, *Sci. Rep.* **2015**, 5, srep15765.
- [38] R.-C. Zhang, D. Sun, R. Zhang, W.-F. Lin, M. Macias-Montero, J. Patel, S. Askari, C. McDonald, D. Mariotti, P. Maguire, *Sci. Rep.* **2017**, 7, 46682.

- [39] N. S. Tabrizi, M. Tazikheh, N. Shahgholi, *Int. J. Green Nanotechnol.* **2012**, *4*, 489.
- [40] G. Sharma, A. Kumar, S. Sharma, M. Naushad, R. Prakash Dwivedi, Z. A. AlOthman, G. T. Mola, *J. King Saud Univ. – Sci.* **2017**.
- [41] D. E. Gheorghe, L. Cui, C. Karmonik, A. Brazdeikis, J. M. Penalzoa, J. K. Young, R. A. Drezek, M. Bikram, *Nanoscale Res. Lett.* **2011**, *6*, 554.
- [42] J. Rick, M.-C. Tsai, B. J. Hwang, *Nanomaterials* **2015**, *6*, 5.
- [43] J. F. Moulder, *Handbook of X-Ray Photoelectron Spectroscopy: A Reference Book of Standard Spectra for Identification and Interpretation of XPS Data*, Physical Electronics Division, Perkin-Elmer Corporation, Eden Prairie, Minnesota **1992**.
- [44] N.d. <http://www.xpsfitting.com>
- [45] R. Hernández, A. Sarafian, D. López, C. Mijangos, *Polymer* **2004**, *45*, 5543.
- [46] T. N. Snyder, K. Madhavan, M. Intrator, R. C. Dregalla, D. Park, *J. Biol. Eng.* **2014**, *8*, 10.
- [47] S. Agnihotri, S. Mukherji, S. Mukherji, *RSC Adv.* **2013**, *4*, 3974.
- [48] C. Han, L. Ge, C. Chen, Y. Li, Z. Zhao, X. Xiao, Z. Li, J. Zhang, *J. Mater. Chem. A* **2014**, *2*, 12594.
- [49] M. P. Mallin, C. J. Murphy, *Nano Lett.* **2002**, *2*, 1235.
- [50] P. Raveendran, J. Fu, S. L. Wallen, *Green Chem.* **2006**, *8*, 34.
- [51] S. Link, Z. L. Wang, M. A. El-Sayed, *J. Phys. Chem. B* **1999**, *103*, 3529.
- [52] B. Zugic, L. Wang, C. Heine, D. N. Zakharov, B. A. J. Lechner, E. A. Stach, J. Biener, M. Salmeron, R. J. Madix, C. M. Friend, *Nat. Mater.* **2017**, *16*, 558.
- [53] M.-J. Kim, H.-J. Na, K. Chul Lee, E. Ah Yoo, M. Lee, *J. Mater. Chem* **2003**, *13*, 1789.
- [54] J.-H. Liu, A.-Q. Wang, Y.-S. Chi, H.-P. Lin, C.-Y. Mou, *J. Phys. Chem. B* **2005**, *109*, 40.
- [55] D. Mariotti, J. Patel, V. Švrček, P. Maguire, *Plasma Process. Polym.* **2012**, *9*, 1074.
- [56] P. Zhao, N. Li, D. Astruc, *Coord. Chem. Rev.* **2013**, *257*, 638.
- [57] J. Patel, L. Němcová, P. Maguire, W. G. Graham, D. Mariotti, *Nanotechnology* **2013**, *24*, 245604.
- [58] A. Henglein, *Chem. Mater.* **1998**, *10*, 444.
- [59] A. Henglein, *J. Phys. Chem.* **1993**, *97*, 5457.
- [60] S. Eckhardt, P. S. Brunetto, J. Gagnon, M. Priebe, B. Giese, K. M. Fromm, *Chem. Rev.* **2013**, *113*, 4708.
- [61] J. Liu, D. A. Sonshine, S. Shervani, R. H. Hurt, *ACS Nano* **2010**, *4*, 6903.
- [62] G. A. Sotiriou, A. Meyer, J. T. N. Knijnenburg, S. Panke, S. E. Pratsinis, *Langmuir* **2012**, *28*, 15929.
- [63] A. Kyrychenko, D. A. Pasko, O. N. Kalugin, *Phys. Chem. Chem. Phys.* **2017**, *19*, 8742.
- [64] T. J. Smith, J. E. Kennedy, C. L. Higginbotham, *J. Mech. Behav. Biomed. Mater.* **2009**, *2*, 264.
- [65] B. Briscoe, P. Luckham, S. Zhu, *Polymer* **2000**, *41*, 3851.
- [66] R. Chen, Q. Chen, D. Huo, Y. Ding, Y. Hu, X. Jiang, *Colloids Surf. B Biointerfaces* **2012**, *97*, 132.
- [67] W. Salem, D. R. Leitner, F. G. Zingl, G. Schratler, R. Prassl, W. Goessler, J. Reidl, S. Schild, *Int. J. Med. Microbiol.* **2015**, *305*, 85.
- [68] H. Le Pape, F. Solano-Serena, P. Contini, C. Devillers, A. Maftah, P. Leprat, *J. Inorg. Biochem.* **2004**, *98*, 1054.
- [69] K. Varaprasad, Y. M. Mohan, S. Ravindra, N. N. Reddy, K. Vimala, K. Monika, B. Sreedhar, K. M. Raju, *J. Appl. Polym. Sci.* **2010**, *115*, 1199.

## SUPPORTING INFORMATION

Additional supporting information may be found online in the Supporting Information section at the end of the article.

**How to cite this article:** Nolan H, Sun D, Falzon BG, et al. Metal nanoparticle-hydrogel nanocomposites for biomedical applications – An atmospheric pressure plasma synthesis approach. *Plasma Process Polym.* 2018;15:e1800112. <https://doi.org/10.1002/ppap.201800112>